



# CHORUS

This is the accepted manuscript made available via CHORUS. The article has been published as:

## Altering the Stability of Surface Plastic Flow via Mechanochemical Effects

Anirudh Udupa, Tatsuya Sugihara, Koushik Viswanathan, and Srinivasan Chandrasekar  
Phys. Rev. Applied **11**, 014021 — Published 10 January 2019

DOI: [10.1103/PhysRevApplied.11.014021](https://doi.org/10.1103/PhysRevApplied.11.014021)

# 1 Altering the Stability of Surface Plastic Flow via Mechanochemical 2 Effects

3 Anirudh Udupa<sup>a,\*</sup>, Tatsuya Sugihara<sup>\*b</sup>, Koushik Viswanathan<sup>a</sup>, Srinivasan Chandrasekar<sup>a</sup>

4 <sup>a</sup>*Center for Materials Processing and Tribology, Purdue University, West Lafayette, IN 47907-2023, USA*

5 <sup>b</sup>*Department of Mechanical Engineering, Osaka University, Suita, Osaka 565-0871, Japan*

---

## 6 **Abstract**

We demonstrate a link between surface plastic flow and ambient chemical environment—a mechanochemical effect—in large-strain deformation of metals, using high-speed *in situ* observations. This link, different from known mechanochemical effects, is studied using aluminum and an alcohol environment. Three distinct flow modes—sinuous, laminar and segmented—occur, depending on the alcohol action on the metal surface. Two transitions, one from sinuous to laminar and the other from sinuous to segmented flow are demonstrated. In both cases, the final flow modes are characterized by smaller deformation forces (order of magnitude) as well as much improved quality of the final surface. The action of the chemical medium itself is coupled to the flow mode, distinguishing it from other mechanochemical effects previously reported. The effect appears to be replicable to different degrees in other metal systems such as copper, iron, stainless steels and nickel. Based on the observations, a schematic stability phase diagram for plastic flow is proposed. Implications of the results for enhancing performance of cutting and surface deformation processes for soft and highly strain-hardening metals are discussed.

7 *Keywords:* metals; large-strain deformation; mechanochemical effect; flow stability;

---

---

\*Corresponding author: audupa@purdue.edu

\*AU and TS made equal contributions to this manuscript

## 8 1. Introduction

9 It has long been appreciated that the nature of mesoscale plastic flow in metals is deter-  
10 mined by considerations of stability [1–4]. The prime and most often cited example in this  
11 regard is, perhaps, the change from uniform homogeneous plastic flow to localized deforma-  
12 tion in the form of shear bands [1, 5]. This example of a homogeneous to non-homogeneous  
13 flow transition occurs in an array of material systems, from rocks on the geological-scale [6]  
14 to structural metals on the mesoscale [5, 7, 8] and to glasses on the nanoscale [9]. However,  
15 the fact that other such transitions may also exist, particularly in large strain deformation,  
16 resulting in flows hitherto poorly understood, is only now beginning to be appreciated [10–  
17 12]. It is quite natural to expect that these transitions can also be explained in terms of  
18 changes in stability, thereby predicting characteristics of the resulting flow.

19 The nature of plastic flow is particularly important in large-strain deformation processes  
20 at or near free surfaces, i.e., unconstrained deformation. The proximity of the free surface  
21 to the deformation zone provides an additional degree of freedom for flow evolution, thereby  
22 being potentially conducive to spawning a rich variety of non-homogeneous flows. A common  
23 feature of these deformation processes is use of intense shear to effect changes in shape,  
24 microstructure and surface properties. Such processes are ubiquitous in materials processing  
25 and manufacturing, encompassing, to name a few, cutting, abrasion, and sliding [13, 14].

26 A related, but well known fact, is that surface plastic deformation is intimately linked  
27 to the environment to which the free surface is exposed to during deformation, as well as  
28 presence of thin surface layers (e.g., oxide films) [15]. For instance, exposing the surface of  
29 certain, otherwise highly ductile, metals to suitable chemical media is known to cause severe  
30 embrittlement, e.g., stress-corrosion cracking and hydrogen/liquid metal embrittlement [16–  
31 18]. These processes too are governed by stability considerations, such as the competition  
32 between continued plastic flow and fracture [19–21].

33 Naturally, given the important consequences of surface flow modes and the potentially  
34 central role of flow stability in determining them, it is of interest to examine the question—  
35 can we induce transitions from one flow mode to another, by utilizing a suitable chemical  
36 environment? This question is pertinent also from a practical point of view, for, driven by  
37 implications for machining, deformation processing and tribology, there is much interest in

38 controlling specific flow modes in surface plasticity [22, 23]. In manufacturing, the flow mode  
39 determines process performance indices like forces, energy consumption, and surface quality.  
40 Likewise, wear processes are closely linked with occurrence of non-homogeneous flow modes  
41 near free surfaces [24–27].

42 In the course of an examination of this question, we discovered that metals can exhibit  
43 widely different flow modes in the presence of suitable chemical media [10, 28]—a sub-class  
44 of phenomena termed mechanochemical effects [22, 29]. Notably, a material independent  
45 mechanochemical effect was found in cutting of ductile and highly strain hardening metals  
46 [28]. By using a chemical medium that physically adheres to the metal’s surface, the type  
47 of plastic flow was fundamentally altered. Based on surface energetics considerations, this  
48 change was shown to resemble a local ductile-to-brittle transition.

49 The present paper describes a different, yet complementary, mechanochemical effect that  
50 is material and chemical medium specific. We use a specially designed system— aluminum  
51 plastically deformed to large strains in an alcohol environment—that demonstrates the intri-  
52 cate coupling between surface plastic flow modes, both homogeneous and non-homogeneous,  
53 and the surrounding chemical environment. The two key features of our system that helped  
54 unearth this coupling are the ductility of Al and its chemical reactivity with alcohols. The  
55 observations provide strong basis for the hypothesis that the plastic deformation mode opera-  
56 tive at surfaces is determined by flow stability considerations. They also suggest possibilities  
57 for beneficially utilizing these effects in cutting and deformation processing of metals. It is  
58 of interest to note here that while the present study is focused on metals, mechanochemical  
59 effects involving solid/liquid state chemical reactions have been exploited commercially in  
60 non-metallic systems, e.g., chemomechanical polishing of Si and ceramics [30–32].

61 The manuscript is organized as follows. Section 2 provides background information on  
62 surface plastic flow modes and the speciality of the aluminum-alcohol system. The details  
63 of the experimental system are discussed in Sec. 3, followed by the results (Sec. 4). We  
64 explain the results within the framework of flow stability and propose a phase diagram for  
65 evaluating stability in the presence of chemical media (Sec. 5). This section also discusses  
66 some implications for manufacturing processes with metals and related avenues for future  
67 work. Concluding remarks are presented in Sec. 6.

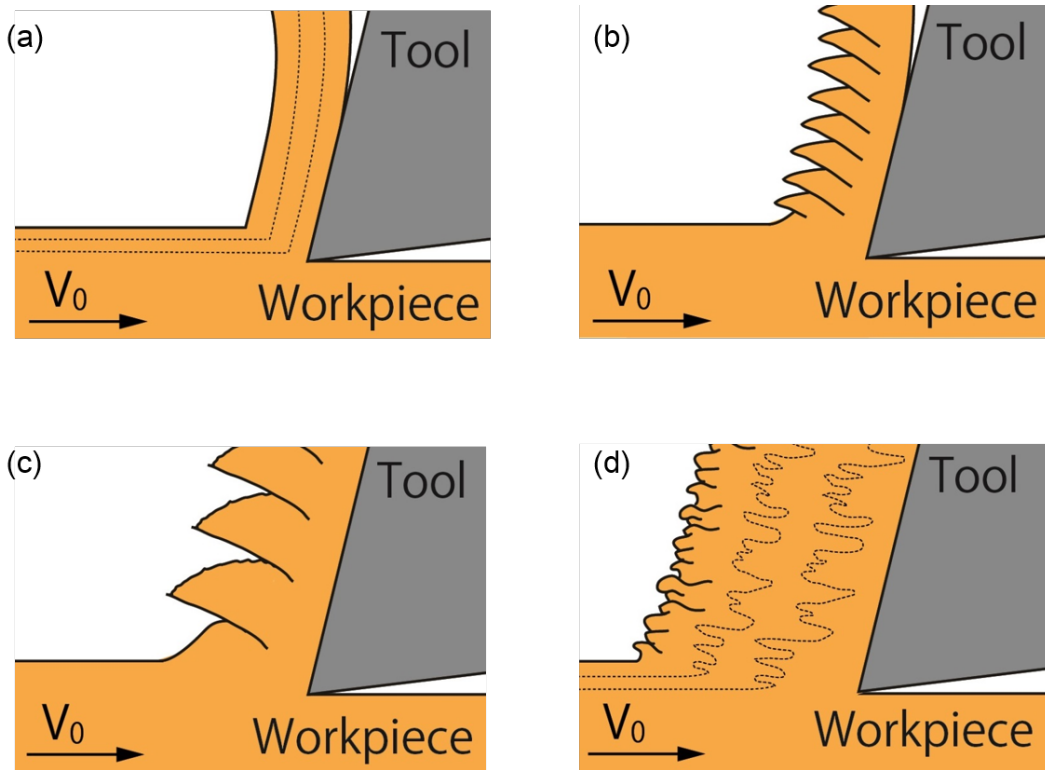


Figure 1: Schematic of four principal plastic flow modes and corresponding chip morphologies in simple shear deformation of metals by cutting. (a) Laminar flow (b) shear band flow (c) segmented flow and (d) sinuous flow. The flow modes may be characterized by the overlaid streakline pattern shown here for modes a) and d).

## 68 2. Background

69 The prototypical mode of plastic flow in large strain deformation is one of steady homo-  
 70 geneous strain, typically with smoothly varying and time-independent strains. In addition,  
 71 three other flow modes have been identified, one until recently unknown, each with their own  
 72 distinct features.

### 73 2.1. Four distinct surface plastic flow modes

74 To best illustrate these flow modes and their features, a prototypical large-strain, simple  
 75 shear deformation geometry is presented in **Fig. 1**, schematically depicting all four flow  
 76 modes. This configuration resembles plane-strain cutting and involves imposition of simple  
 77 shear on a moving workpiece using a sharp wedge-shaped tool. The shearing process removes  
 78 a thin layer of material from the workpiece, the chip, see **Fig. 1**. The four flow modes result  
 79 in distinct morphologies in the chip, a fact that has only recently begun to be appreciated

80 based on combined *in situ* and *ex situ* analyses [11, 12, 33], even though chip morphologies  
81 themselves have been studied for a long time [5, 13, 34–36]. The four modes are: 1) steady  
82 homogeneous deformation, henceforth referred to as laminar flow (**Fig. 1(a)**); 2) shear band  
83 flow, with periodic deformation restricted to very narrow zones [1, 3, 5], as in **Fig. 1(b)**;  
84 3) segmented flow characterized by non-uniform deformation and periodic fracture, as in  
85 **Fig. 1(c)**; and 4) the more recently uncovered sinuous flow, typified by surface (plastic)  
86 buckling, material folding, and highly non-homogeneous straining (**Fig. 1(d)**) [10, 11]. The  
87 latter three modes, being non-homogeneous and unsteady, will be referred to as non-laminar  
88 flow modes. *In situ* and *ex situ* observations [12] have established that these different flow  
89 modes result in chips with characteristic morphologies (signatures), see **Fig. 1**. Similar flow  
90 modes and wear particle morphologies have also been observed in sliding, another well-known,  
91 large-strain deformation process [27].

## 92 *2.2. Role of stability*

93 This rich diversity of flow modes in cutting and sliding is a direct consequence of the  
94 presence of the free surface, and is quite distinct from the more limited flow patterns typical  
95 of constrained deformation processes like bulk metal forming [37]. Which of these flow  
96 modes actually occurs in a certain situation is determined by stability criteria, including  
97 considerations of surface plastic buckling [33], crack growth from free surface flaws [15, 38] as  
98 well as the material’s inherent propensity to exhibit flow localization [3]. In manufacturing  
99 and materials processing, a large body of evidence exists to show that the flow mode and  
100 stability of flow are strongly influenced by the initial deformation state of the metal (e.g.,  
101 annealed, pre-strained) and deformation geometry (e.g., die angle) [13, 37]. Furthermore,  
102 the presence of specific chemical environments is known to introduce additional constraints  
103 on flow stability, by promoting auxiliary processes such as crack nucleation and growth  
104 [22, 23, 39].

## 105 *2.3. Aluminum and its reactivity with alcohols — a model system*

106 The use of Al and alcohols as a model system for studying chemical environment effects  
107 on surface plastic flow has three primary advantages.

108 Firstly, commercially pure aluminum, based on the initial deformation state of its surface,  
109 is known to demonstrate at least 3 of the 4 flow modes discussed in **Fig. 1** [11, 40]. Therefore,  
110 using this metal for studying large strain deformation allows us, in principle, to probe the  
111 effect of a chemical environment on multiple flow modes within the same material system.

112 Secondly, fresh Al surfaces readily react with alcohols to form alkoxides, an important  
113 class of compounds characterized by aluminum-oxygen-carbon bonding [41]. Industrially,  
114 alkoxides such as isopropoxide and sec-butoxide are important for production of ketones and  
115 aldehydes, where they are employed as reducing agents [42]. When a fresh Al surface reacts  
116 with isopropyl alcohol, the resulting aluminum isopropoxide formed is a white solid (melting  
117 point 118° C), otherwise usually prepared by an elaborate synthesis method via formation  
118 of an amalgam [43].

119 Thirdly, alcohols and the resulting alkoxides can be effective lubricants [44–47]. The  
120 lubrication is claimed to be effected by a negative-ion-radical mechanism that changes the  
121 interface conditions during sliding [48].

122 Thus the Al-alcohol system offers much scope for altering the nature of the shear de-  
123 formation at surfaces (e.g., **Fig. 1**), both via formation of alkoxide layers to effect surface  
124 energy changes and via lubricant films to change the friction at and near the deformation  
125 zones.

### 126 **3. Experimental Details**

127 Large strain deformation is imposed using the model framework of a workpiece sliding  
128 at constant velocity  $V_0$  against a rigid wedge (tool/die), see **Fig. 2**. As the workpiece is  
129 pushed against the wedge/tool, a thin layer of material, of initial thickness  $h_0$ , is continuously  
130 deformed under simple shear and removed as a ‘chip’ of thickness  $h_C$ , with a fresh surface  
131 created on the workpiece. The ratio  $\lambda = h_C/h_0$  is typically between 2 and 20, depending on  
132 the underlying flow mode [11, 12, 33, 36]. This configuration, analogous to cutting, is well-  
133 characterized in terms of loading and chip deformation [13]. For the experiments described  
134 in this manuscript,  $V_0$  was fixed at 5 mm/s. The low speed ensures that thermal effects on  
135 the deformation are minimal: **for these conditions, the temperature change was estimated**  
136 **to be  $< 5^\circ\text{C}$**  [13]. The undeformed chip thickness ( $h_0$ ) value was set nominally at 50  $\mu\text{m}$

137 in the experiments. However, due to compliances in the tool and work holding system, it  
138 was difficult to exactly achieve this set value. In practice, we used iterative adjustment of  
139 the  $h_0$  setting to get an actual value that was close to the targeted value. The exact  $h_0$  in  
140 the experiments was measured both from the images and by utilizing a dial indicator; these  
141 values were respectively 55  $\mu\text{m}$ , 49  $\mu\text{m}$  and 53  $\mu\text{m}$  for the dry cutting, IPA and alkoxide  
142 cutting experiments, respectively.

### 143 3.1. Workpiece and tool properties

144 The tool was made of a commercial grade WC-Co alloy, with cutting edge width of 2.3  
145 mm (equal to chip width), edge radius of  $< 5 \mu\text{m}$ , and rake angle  $\alpha = 10^\circ$  (**Fig. 2**). The  
146 workpiece was commercially pure Al (Al 1100, dimensions 75 mm length  $\times$  25 mm height  
147  $\times$  6 mm width). The workpiece was prepared in an initially annealed state, by heating in a  
148 furnace at 550°C for 4 hours and then furnace-cooling to room temperature. The reason for  
149 using aluminum in the annealed condition was because in this state it is soft and ductile, and  
150 exhibits unsteady sinusoidal via plastic buckling while cutting [33]. This enables examination  
151 of unsteady and, potentially, multiple flow modes within the same material system.

### 152 3.2. In-situ characterization of surface plastic flow modes

153 Plastic flow in the deformation zone during chip formation was recorded *in situ* using  
154 a high-speed CMOS camera (PCO dimax) coupled to a long working distance microscope  
155 objective, see **Fig. 2**, right. The deformation zone was illuminated using a 150 W halogen  
156 lamp. A glass block was clamped against the side face of the workpiece to constrain the  
157 deformation to remain plane-strain, see **Fig. 2**. Images were captured at 500 frames per  
158 second and spatial resolution of 1.4  $\mu\text{m}$  per pixel. The image sequences were analyzed  
159 using a digital image correlation technique—Particle Image Velocimetry (PIV)—to obtain  
160 quantitative details of flow, such as effective (von Mises) strain and strain rate fields, and  
161 flow line patterns [10]. This data enabled detailed mapping of the underlying surface plastic  
162 flow modes.

163 Concurrently, forces on the tool, both parallel (cutting force  $F_c$ ) and perpendicular (thrust  
164 force  $F_t$ ) to  $V_0$  were recorded using a mounted piezoelectric dynamometer (Kistler 9272, nat-  
165 ural frequency  $\sim 2$  kHz). The cutting force  $F_c$  is the primary contributor to the deformation



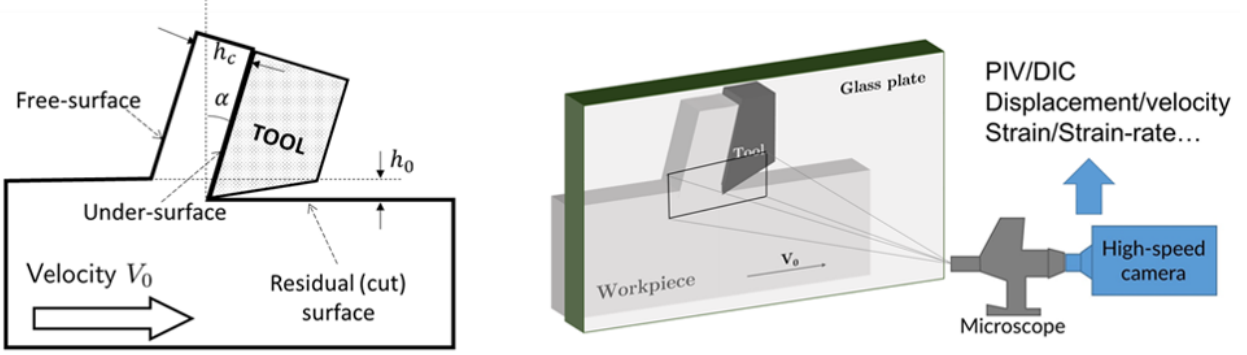


Figure 2: Schematic of plane-strain cutting used to impose simple-shear deformation in chip and high-speed imaging conguration used to characterize flow patterns. (Left) Notation defining deformation geometry ( $\alpha, h_0, h_C$ ) and various surfaces of workpiece and chip (free surface, under-surface and cut surface). (Right) The deformation zone is observed in-situ to obtain quantitative flow field information at high resolution.

166 energy/power since it is oriented parallel to  $V_0$  [13]. From these components, the resultant  
 167 force was obtained, as well as the force components parallel ( $F_f$ ) and perpendicular ( $F_n$ ) to  
 168 the tool face in contact with the chip. Since the actual  $h_0$  values were slightly different for  
 169 each of the three experimental conditions (dry, IPA and alkoxide), the forces were normalized  
 170 by dividing by  $h_0$  to obtain specific force values ( $\bar{F}_c = F_c/h_0, \bar{F}_t = F_t/h_0$ ) for each of the  
 171 conditions. The specific force values and specific energy are used to characterize and analyze  
 172 the energy dissipation corresponding to the three conditions (flow modes).

173 The topography of the cut (residual) surface in the wake of the tool was characterized  
 174 using an optical profilometer (Zygo NewView 8300) to obtain surface roughness data, and  
 175 details of defects such as tears and cracks.

### 176 3.3. Role of chemical environment

177 A series of cutting experiments was carried out within the framework of **Fig. 2** to examine  
 178 how the chemical environment in the vicinity of the workpiece and chip surface, influenced  
 179 the plastic flow modes. The reactivity of a freshly generated Al surface with isopropyl alcohol  
 180 (henceforth IPA), coupled with the lack of reactivity between IPA and an oxide-covered Al  
 181 surface, allowed four different chemical conditions to be studied, see **Fig. 3**:

- 182 1. **Dry cutting, Fig. 3(a)**: In the first series of experiments, the cutting was performed  
 183 without use of IPA or any other fluid.
- 184 2. **IPA cutting, Fig. 3(b)**: In a second series of experiments, the tool-workpiece region

185 was flooded with commercially available IPA. In this ambient condition the tool-chip  
186 contact interface is altered due to the formation of a layer of aluminum isopropoxide  
187 (alkoxide) on the chip under-surface, facilitated by the freshly generated oxide-free  
188 Al surface. Absent such an oxide-free surface, this reaction between aluminum and  
189 IPA needs either the presence of a catalyst or high temperatures to overcome the  
190 natural oxide layer. **Figure 3(b)** indicates locations where alkoxide is formed as freshly  
191 exposed aluminum comes in contact with IPA. The alkoxide layer thus formed acts as  
192 a lubricating film at the tool-chip contact (see Sec. 2).

193 **3. Alkoxide cutting, Fig. 3(c):** A third series of cutting experiments was performed by  
194 cutting without any IPA at all, but with an alkoxide film on the workpiece free surface,  
195 remote from the tool-chip contact zone. This film is formed as follows. The IPA cutting  
196 (above), besides altering the chip under-surface, leaves behind an alkoxide layer along  
197 the entire length of the residual (cut) surface, see **Fig. 3(b)**. This is because the  
198 freshly generated and oxide-free cut surface, being highly reactive, forms an alkoxide  
199 film with continuous exposure to the IPA. Now performing a second cutting pass over  
200 this newly created surface on the same workpiece (identical  $h_0, V_0$ ) amounts to cutting  
201 a workpiece with a thin alkoxide film on its free surface. Since the residual strain on  
202 the workpiece surface after IPA cutting was small,  $< 0.4$  as estimated by PIV, the flow  
203 in the alkoxide cutting was found to be negligibly influenced by this residual strain.  
204 This was confirmed in multiple experiments. A discussion of residual strain effects on  
205 the cutting flow mode can be found in Ref. [11]

206 **4. IPA + Alkoxide cutting, Fig. 3(d):** A fourth series of cutting experiments was  
207 performed wherein an alkoxide film was present on both the initial workpiece free  
208 surface as well as the chip under surface. For this purpose, the cutting was done as in  
209 the alkoxide cutting case, but with the tool-workpiece region flooded with IPA.

## 210 4. Results

211 The high-speed, *in situ* observations have captured flow modes in three different chemical  
212 environments, that highlight the influence of chemical media on stability of surface plastic

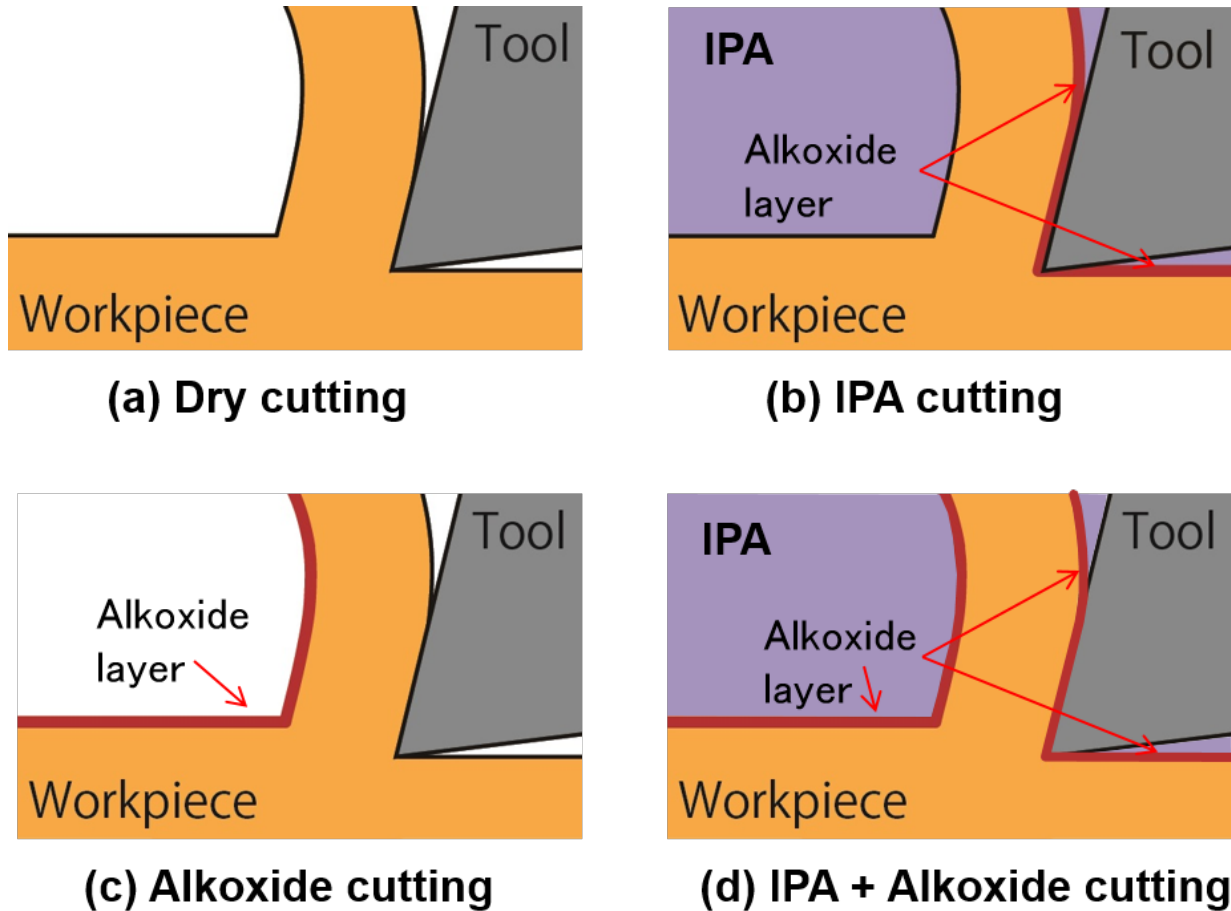


Figure 3: Description of four different chemical ambient conditions used in cutting experiments with annealed Al. (a) Dry cutting: Cutting of annealed Al without use of any medium. (b) IPA-cutting: Annealed Al is cut in a bath of IPA. As a consequence, the chip under-surface and newly generated workpiece surface in wake of the wedge tool are both directly exposed to the IPA soon after these surfaces are created. Alkoxide layer is formed on both the chip under-surface and the residual (cut) surface in wake of the wedge. This provides a means of probing plastic flow modes and flow stability by action of IPA only along the chip under-surface. (c) Alkoxide cutting: Annealed Al, with alkoxide layer on its free surface, is cut without use of any medium. This condition provides a means of probing flow stability when only the initial workpiece surface is coated with an alkoxide layer. (d) IPA + Alkoxide cutting: Cutting with alkoxide layer formed on both the free surface as well as on the chip under-surface. This condition provides a means of probing flow stability when there is an alkoxide layer on both surfaces.

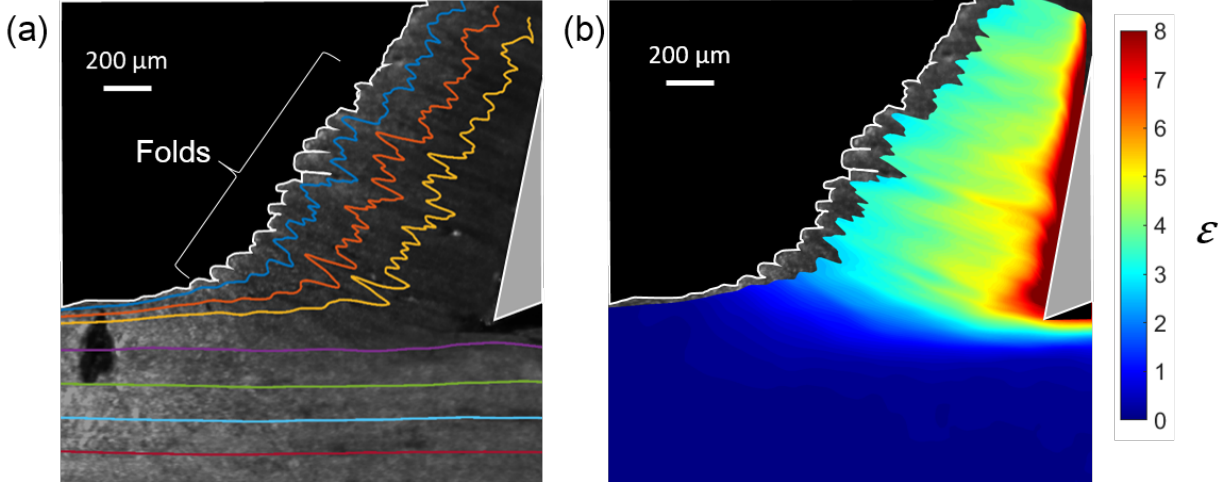


Figure 4: Flow pattern and deformation in dry cutting. (a) Image from a high-speed sequence with superimposed streaklines from PIV. The highly wavy streaklines are characteristic of folding and sinuous flow. (b) The strain distribution is highly non-homogeneous due to the folding. The ratio ( $\lambda = h_C/h_0$ ) of deformed to undeformed chip thickness is 19, indicating extreme thickening of the chip and deformation. Note the mushroom-like structures on the free surface of the chip which are typical of sinuous flow.  $V_0 = 5$  mm/s and  $h_0 = 55$   $\mu\text{m}$ .

213 flow. The results from these direct observations were complemented/reinforced by concurrent  
 214 measurements of force, energy and cut-surface quality.

#### 215 4.1. Dry cutting

216 In the absence of any chemical (IPA), annealed Al deforms via sinuous flow under the  
 217 chosen conditions; a typical chip is shown in **Fig. 4**. The chip is extremely thick, with  
 218 the ratio  $h_C/h_0 \simeq 19$ ; indicative of large underlying strains. Sinuous flow, a non-laminar  
 219 flow mode, is characterized by large amplitude folding in the material, as revealed by the  
 220 streaklines overlaid in **Fig. 4(a)**. This type of flow is quite common in cutting of annealed  
 221 and/or highly strain-hardening metals [10, 11, 33]. **Figure 4(b)** shows the effective (von  
 222 Mises) strain in the chip, obtained from PIV. The chip strain distribution is quite non-  
 223 homogeneous, reflecting the repeated folding, and alternates between high ( $\approx 6$ ) and low  
 224 ( $< 3$ ) values. The folding also causes the free surface of the chip to have an irregular  
 225 morphology with mushroom-like structures (**Fig. 4**). This morphology is typical of sinuous  
 226 flow, as seen in other metals like Cu and Fe.

227 Sinuous flow is initiated by plastic buckling of a thin surface layer ahead of the tool.  
 228 Details of this flow development and its microstructure origins have been discussed in prior

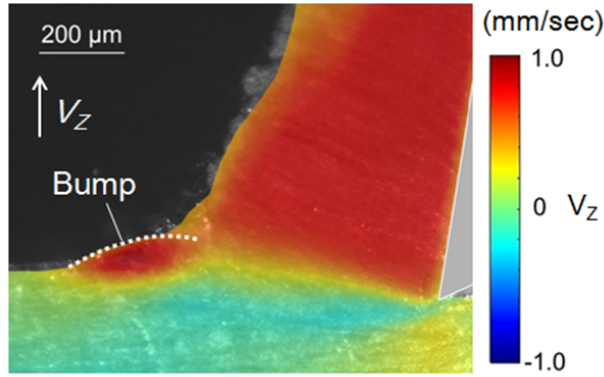


Figure 5: Velocity distribution in vertical direction ( $V_Z$ ) in dry cutting. Bump formation is confirmed on the free surface by the sharp contrast between  $V_Z$  in bump relative to surrounding material.

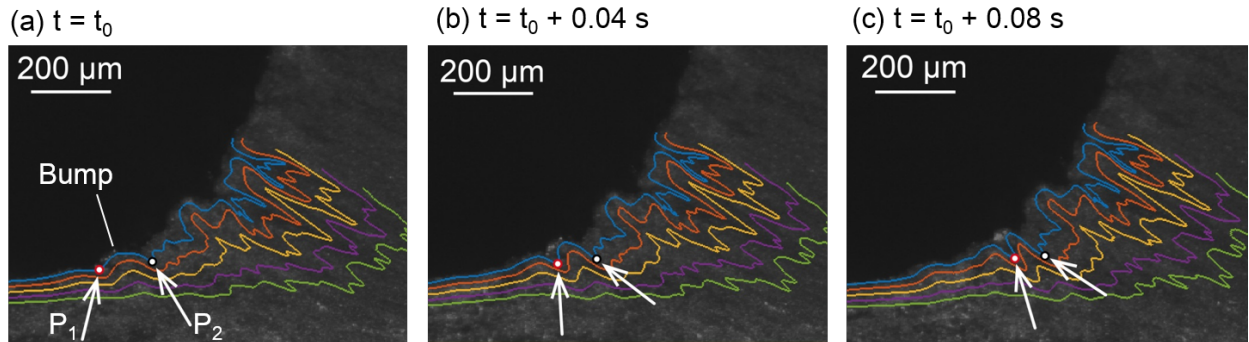


Figure 6: Development of sinuous flow in dry cutting as captured by three frames from a high-speed sequence. (a) A bump is formed due to a plastic buckling instability between pinning points  $P_1$  and  $P_2$ , ahead of the chip. The arrows track the positions of these pinning points in the frames. (b), (c) The bump grows in size (amplitude) and evolves into a fold, resulting in the wavy streaklines.

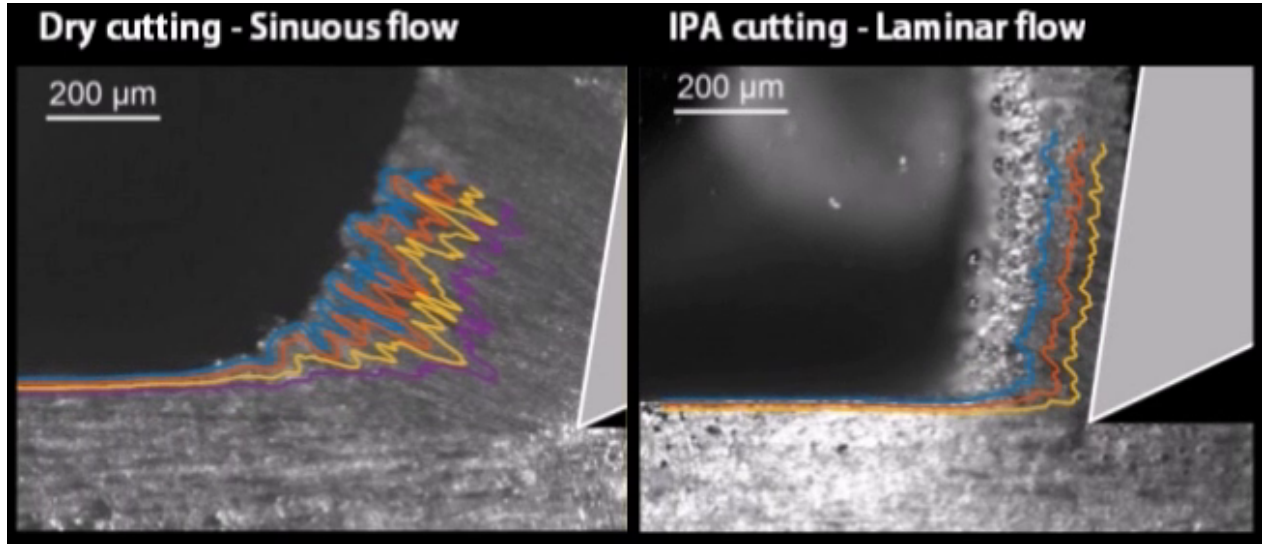
229 work [10, 11, 33], and may be summarized as follows. During sinuous flow, the material  
 230 demonstrates repeated large-amplitude folding. Each folding event is initiated by the forma-  
 231 tion of a protuberance or a bump on the free surface, resulting from plastic buckling. This  
 232 bump formation is shown in **Fig. 5**, using the  $z$ -component of the material velocity ( $V_Z$ ),  
 233 derived from PIV.  $V_Z$  in the chip (0.8 mm/s) is naturally greater than that in the workpiece  
 234 (0 mm/s,  $V_0$  horizontal). The zone where the bump forms has a pronounced  $V_Z$  in contrast  
 235 to the surrounding material. The subsequent evolution of this bump into a fold is shown in  
 236 the image sequence of **Fig. 6**. The initial bump is constrained between two material points  
 237 (termed pinning points  $P_1$  and  $P_2$ , see at arrows) of minimal local curvature (frame 1). As  
 238 the tool advances, these pinning points approach each other (frame 2) and the bump grows,  
 239 evolving into a large-amplitude fold (frame 3). This process then repeats with the folds  
 240 stacking up closely on top of one another to form the thick chip ( $\lambda = 19$ ). **Each of the folds**  
 241 **appears like a mushroom-shaped feature on the chip free surface [50] and the region between**  
 242 **adjacent folds resembles a notch [28].**

#### 243 4.2. IPA cutting

244 The large-amplitude folding and sinuous flow that accompany dry cutting result in very  
 245 high cutting forces and a very thick chip. In sharp contrast, the chip formed in IPA cutting  
 246 (*cf.* **Fig. 3**) was significantly thinner ( $\lambda = h_C/h_0 \simeq 4.8$ ) than with dry cutting ( $\lambda = 19$ ).  
 247 Most strikingly, as seen in **Fig. 7**, the flow was homogeneous and laminar, as revealed by  
 248 the smooth streaklines (see **Movie S1**). No folding is observable on the macroscale, and the  
 249 mushroom-like morphology (*cf.* **Fig. 4**) is also absent on the chip free surface. Additionally,  
 250 the strain-field in IPA cutting is homogenous throughout the chip (**Fig. 7(b)**), with much  
 251 smaller maximum strain ( $\sim 3$ ). The strain increases in a narrow region between the workpiece  
 252 and chip, indicative of intense shear within a narrow zone ('a shear plane'), similar to the  
 253 chip in **Fig. 1(b)**. This laminar flow mode is what is usually seen in many large-strain, shear  
 254 deformation conditions with moderately pre-strained metals [34, 51, 52].

255 This transition in the flow from sinuous to laminar, with the same material and deforma-  
 256 tion geometry, is due to the lack of any buckling on the free surface in the IPA cutting. Many  
 257 alcohols, including IPA, are known to be effective lubricants for aluminum under conditions  
 258 when a stable alkoxide layer is established on the Al surface [44].





Movie S1: Comparison of dry cutting and IPA cutting. Dry cutting of annealed Al (left) results in sinuous flow, thick chip and a large cutting force. IPA cutting (right), on the other hand, results in a relatively smooth laminar flow, thin chip and a much smaller cutting force.

259 In the present experiments, existence of the alkoxide layer, on both the free surface and  
 260 chip under-surface, was detected using Fourier transform infra-red spectroscopy (FTIR).  
 261 Specifically, absorbance peaks were detected in the  $2840 - 3000 \text{ cm}^{-1}$  and the  $1720 - 1740$   
 262  $\text{cm}^{-1}$  ranges, indicating the presence of  $C - H$  and  $C = O$  bonds in the layer. It is expected  
 263 that the thickness of the alkoxide layer so formed is  $\sim 15 \text{ nm}$  [49]. In contrast, no alkoxide  
 264 film was detected on the uncut workpiece free surface ahead of the tool due to the presence  
 265 of the natural oxide layer on the Al. Thus, the IPA cutting condition is ideal for examining  
 266 the effect of a lubricant film (here alkoxide) on the plastic flow modes.

267 The importance of this alkoxide layer in lowering tool-chip friction and cutting forces,  
 268 thereby reducing the propensity for surface buckling and folding, is discussed in Sec. 4.5.

### 269 4.3. Alkoxide cutting

270 When compared to the dry cutting, the alkoxide-cutting (see **Fig. 3(c)**) also produced  
 271 a much thinner chip ( $\lambda = 6.7$ , **Fig. 8**); this chip is only slightly thicker than in the IPA-  
 272 cutting ( $\lambda = 4.8$ ). Surprisingly, however, the flow mode by which this thin chip formed was  
 273 fundamentally different from the laminar flow of IPA cutting and, of course, also from the  
 274 sinuous flow of dry cutting. **Figure 8(a)** shows the streakline pattern and characteristic  
 275 attributes of this flow mode—segmented flow—derived from the high-speed imaging, while

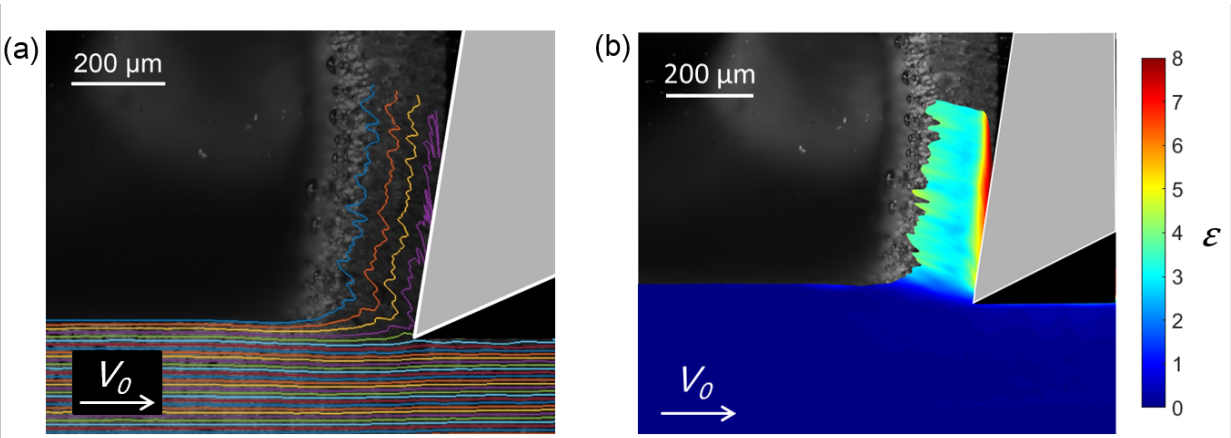


Figure 7: Flow pattern and deformation in IPA-cutting. (a) Image from a high-speed sequence with superimposed streaklines. The relatively smooth streaklines are indicative of laminar flow. (b) The strain distribution is now homogeneous.  $\lambda = h_C/h_0$  is equal to 4.8, much smaller than in the sinuous flow case.  $V_0 = 5$  mm/s and  $h_0 = 49$   $\mu\text{m}$ .

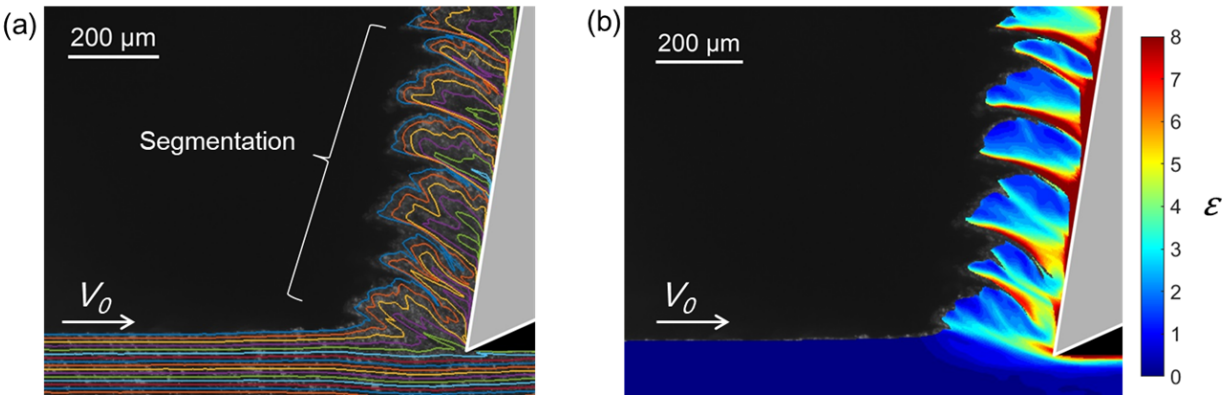


Figure 8: Flow pattern and deformation in alkoxide cutting. (a) Image from a high-speed sequence with superimposed streaklines showing segmented flow. The alkoxide layer on free surface of chip/workpiece changes the flow mode from sinuous to segmented. Cracks nucleate periodically on chip free surface and propagate toward the tool tip, giving rise to the segmented flow topology. (b) The (von Mises) strain is once again inhomogeneous reflecting the nature of the deformation.  $V_0 = 5$  mm/s and  $h_0 = 53$   $\mu\text{m}$ .



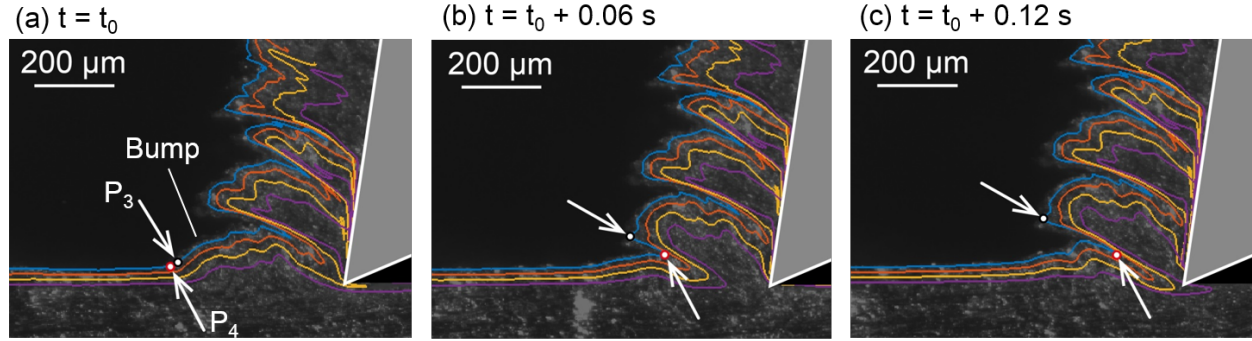
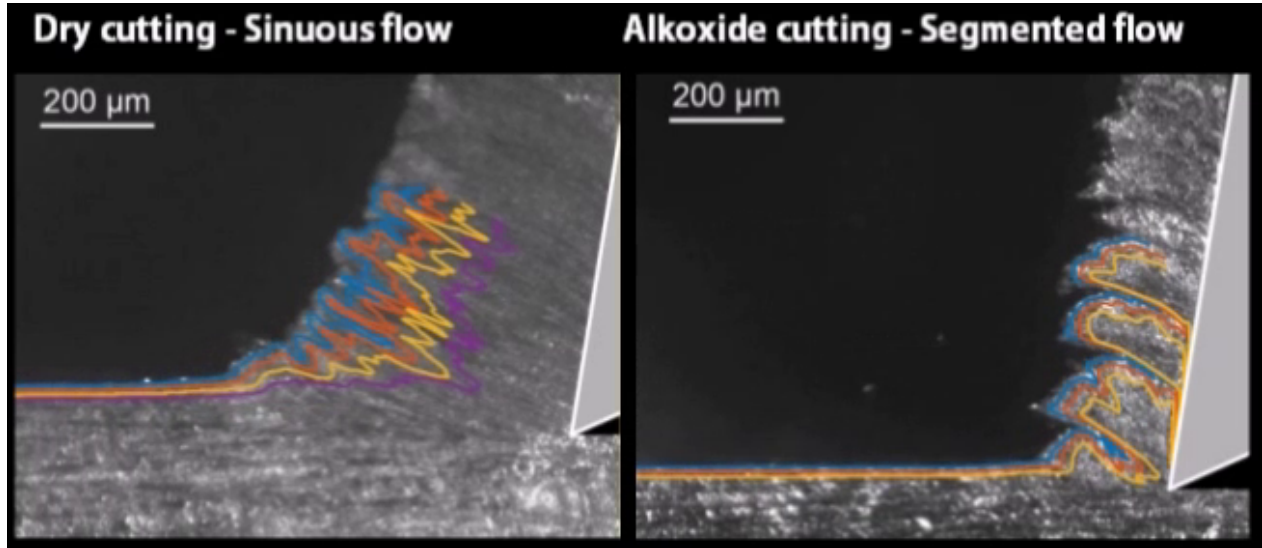


Figure 9: Development of segmented flow in alkoxide cutting as captured by three frames from a high-speed sequence. (a) A bump is formed on the free surface as in dry cutting.  $P_3$  and  $P_4$  show two neighboring (pinning) points in the bump region. (b) In contrast to dry cutting, the bump does not develop into a fold. Instead, a crack nucleates between the points  $P_3$  and  $P_4$  shown at arrows. (c) The crack propagates towards the tool tip as indicated by the increasing distance between these points.

276 **Fig. 8(b)** shows the corresponding strain field. The streaklines indicate the highly unsteady  
 277 nature of the deformation, but their pattern is quite different from that in the sinuous flow (*cf.*  
 278 **Fig. 6** and **Movie S2**). The chip strain distribution is highly non-homogeneous (**Fig. 8(b)**),  
 279 with a strain of  $\sim 2$  for the most part of the chip, interspersed with much higher strain regions  
 280 (strain 7 – 8) of narrow width near the cracks. Segmented flow has in the past been observed  
 281 in cutting of metals of limited ductility like  $\beta$ -brass, hard steels and highly pre-strained metals  
 282 [13]. The manifestation of this flow mode in annealed Al, which is at the other extreme of  
 283 the ductility spectrum, is therefore a strong indication that its surface has been ‘embrittled’  
 284 by chemical reaction with the IPA. This is most likely because of alkoxide formation on the  
 285 workpiece surface facilitated by the specific conditions of the alkoxide cutting experiment  
 286 (**Fig. 3(c)**).

287 The embrittling effect of the alkoxide on the free surface is evident in the periodic cracks  
 288 that initiate on the free surface leading to individual segments. This process can be described  
 289 using the three frames from a high-speed sequence shown in **Fig. 9**. A protuberance or bump,  
 290 resembling the one initiating sinuous flow (**Fig. 6**), is formed, again by plastic buckling, see  
 291 frame 1. Two neighboring material points in the bump region are highlighted in this frame  
 292 (black and red dots). The evolution of a single segment can be inferred from the motion  
 293 of these points, which eventually end up on opposite sides of a cracked surface. As the  
 294 workpiece moves against the tool, the size of the bump does not increase to form a fold as in



Movie S2: Comparison of dry cutting and Alkoxide cutting. Dry cutting of annealed Al (left) results in sinuous flow, thick chip and a large cutting force. Alkoxide cutting (right), albeit still unlubricated, results in a segmentation-type flow, with cracks forming periodically and a much reduced cutting force.

295 sinuous flow. Instead, a crack initiates at one of the pinning points and propagates from the  
 296 workpiece surface (or free surface of the incipient chip) towards the tool tip. The propagation  
 297 of this crack is reflected in the increased distance between the marked points in frame 2. The  
 298 crack propagates to varying distances, depending on the cutting conditions ( $h_0$ ,  $\alpha$ ,  $V_0$ ), before  
 299 it is arrested (frame 3). Subsequently, another plastic buckling event occurs leading to a  
 300 protuberance and cracking at a pinning point, and the process repeats. In other words,  
 301 sinuous flow is disrupted in the incipient folding stage itself by recurring crack formation  
 302 leading to segmented flow.

303 These *in situ* observations of the transition from sinuous flow to segmented flow (*cf.*  
 304 **Fig. 1**) show that the presence of the alkoxide on the free surface of the chip increases the  
 305 propensity for a crack to nucleate and propagate. The incipient folds, caused by the surface  
 306 buckling, provide precursor defects like notches, wherein the chemical action causes local  
 307 crack nucleation via changes to the metal's surface energy. Thus, it is only when the free  
 308 surface of the metal is chemically altered that the sinuous flow transitions to segmented flow.  
 309 This 'mechanochemical' action of the IPA via the alkoxide surface layer thus appears to be  
 310 strongly coupled to the prevailing flow mode: incipient sinuous flow favors this action with  
 311 segmentation ensuing, while laminar flow does not. This type of effect wherein the chemical

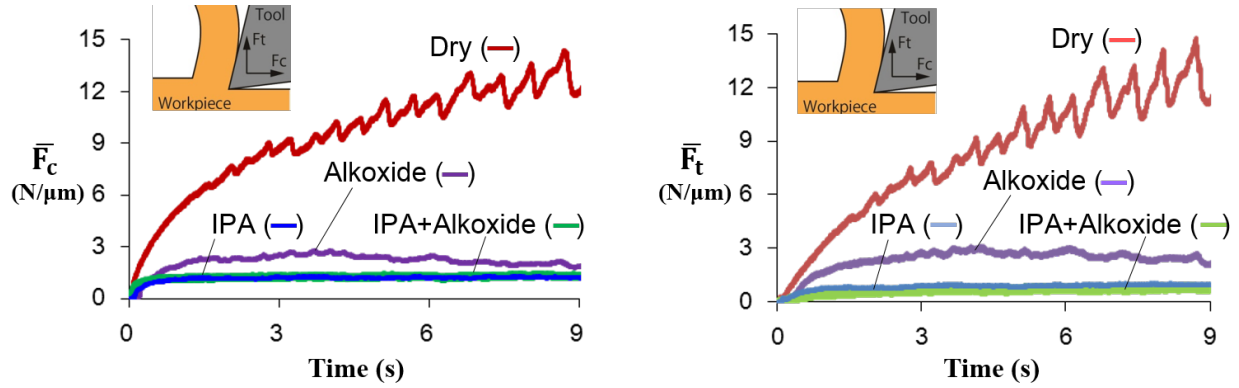


Figure 10: Specific force ( $\bar{F} = F/h_0$ ) in shear deformation under various cutting conditions (dry, IPA and alkoxide). (a) Specific cutting force ( $\bar{F}_c$ ) and (b) specific thrust force ( $\bar{F}_t$ ).  $\bar{F}_c$  and  $\bar{F}_t$  in IPA-cutting are smaller by an order of magnitude compared to dry cutting, whereas the specific forces in alkoxide cutting are smaller by a factor of 6 relative to dry cutting. The specific forces in that case of IPA+Alkoxide cutting is identical with IPA cutting.

312 action of the medium is coupled to the flow mode is quite different from previously reported  
 313 mechanochemical effects in surface plasticity [19, 20, 39].

314 Given that the alkoxide layer can induce two different plastic flow modes depending on  
 315 which surface it is present on, a natural question is the following: what would be the flow  
 316 mode when an alkoxide layer is present on both the free surface as well as on the chip  
 317 under-surface? The answer to this question was obtained from the IPA+Alkoxide cutting  
 318 experiment (**Fig. 3(d)**). In this experiment, the flow was laminar and the chip strain was  
 319 homogenous, with  $\lambda = 4.9$ . In fact, this flow was essentially indistinguishable from the flow  
 320 in the IPA cutting in every respect. Hence, it is clear that whenever an alkoxide lubricant  
 321 film is present at the tool-chip interface, laminar flow will always be the dominant flow mode.  
 322 This is irrespective of whether an alkoxide layer is present on the chip free surface. Further  
 323 implications of this result are discussed in Sec. 5

#### 324 4.4. Forces and energy consumption

325 Measured force components under all three chemical conditions are shown in **Fig. 10**.  
 326  $F_c$  (**Fig. 10(a)**) and  $F_t$  (**Fig. 10(b)**) represent the cutting (parallel to  $V_0$ ) and thrust forces  
 327 (normal to  $V_0$ ) respectively, while  $\bar{F}_c$  and  $\bar{F}_t$  represent the forces normalized with respect to the  
 328 actual undeformed chip thickness. In dry cutting, both components show a gradual increase  
 329 to steady state, at which stage  $\bar{F}_c \simeq 12N/\mu\text{m}$ . This force value is quite high even though  
 330 the material being cut is soft Al (23 HV)—a consequence of the large thickness change and

331 deformation occurring in the workpiece material as it is converted into the chip, see **Fig. 4**  
 332 ( $\lambda = 19$ , strain 5 – 7). It is also worth noting that the friction force (component along the  
 333 tool face)  $F_f$  is 1.6 times  $F_n$ . If we define a friction coefficient ( $\mu$ ) for the tool-chip contact as  
 334 the ratio of  $F_f/F_n$ , then  $\mu = 1.6$ . In cutting of metals, this  $\mu$  can assume values greater than  
 335 unity [13]. It must be cautioned however that  $\mu$  is more like a pseudo friction coefficient; for  
 336 in cutting its value is influenced also by the tool rake angle, rather than being determined  
 337 completely by the chip and tool materials in contact, and the lubrication condition.

338 In the laminar IPA cutting, both  $\bar{F}_c$  and  $\bar{F}_t$  were around 1.2 N/ $\mu\text{m}$ , an order of magnitude  
 339 smaller than those of the sinuous flow mode of dry cutting (**Fig. 10**). Using  $F_c$ , the specific  
 340 energy (energy per unit volume of material removed) can be calculated as,

$$U = \frac{F_c V_0}{V_0 b h_0} = \frac{F_c}{b h_0} \quad (1)$$

341 where  $b$  is the width of cut. Since  $F_c$  is a direct measure of the specific energy in cutting, the  
 342 IPA cutting occurs with much smaller energy consumption ( $U_{IPA} \sim 0.53 \text{ J/mm}^3$ ) compared  
 343 to the dry cutting case ( $U_{dry} \sim 4.65 \text{ J/mm}^3$ ). This is undoubtedly a consequence of the much  
 344 smaller deformation imposed. Furthermore, unlike with the sinuous flow,  $F_c$  and  $F_t$  reached  
 345 their steady values much more quickly for the laminar flow mode. The tangential force,  $F_t$ ,  
 346 along the tool face in the IPA cutting was also an order of magnitude smaller than in dry  
 347 cutting case. Since this force is a measure of the frictional drag at the tool-chip contact, it  
 348 shows that the IPA action at this contact has also reduced the frictional energy dissipation  
 349 (secondary deformation) considerably. The change in friction can be inferred from the value  
 350 of  $\mu = 0.9$ , significantly different from the dry cutting ( $\mu = 1.6$ ).

351 The IPA+Alkoxide cutting case was indistinguishable from the IPA cutting case, not just  
 352 from the flow mode but even from the specific forces. Even the value of  $\mu = 0.8$  is very close  
 353 to the IPA cutting case. The observations strongly suggest that the friction force reduction  
 354 in IPA cutting as well as the IPA + Alkoxide cutting has stabilized the laminar flow mode  
 355 vis-à-vis sinuous flow, by inhibiting the surface buckling.

356 In the case of alkoxide cutting, the forces and specific energy are again much smaller  
 357 ( $\bar{F}_c \sim 2 \text{ N}/\mu\text{m}$ ,  $U_{alkoxide} \sim 0.87 \text{ J/mm}^3$ ) than in the sinuous flow case, an almost 80%

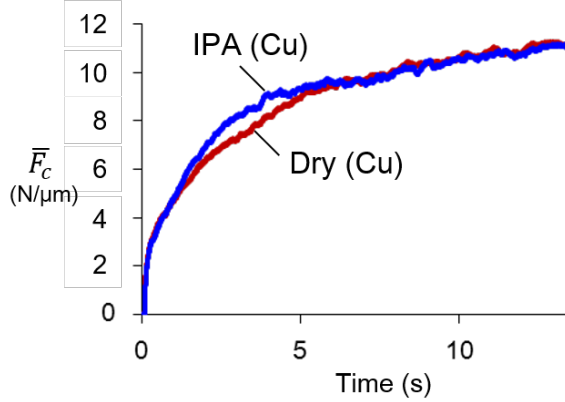


Figure 11: Specific cutting force in annealed Cu for dry and IPA cutting ( $\alpha = 0^\circ$ ,  $h_0 = 50 \mu\text{m}$ ,  $V_0 = 5 \text{ mm/sec}$ ). In contrast to the Al cutting, IPA has no effect on cutting force in the Cu. This strongly suggests that lubrication in the Al is not because of the alcohol itself but due to the formation of an alkoxide layer along the chip under-surface.

358 decrease, see **Fig. 10**. This large decrease is, at first sight, surprising since both conditions  
 359 are essentially unlubricated, i.e., without any IPA access to the tool-chip interface. The  
 360 unlubricated condition can be inferred from the value of  $\mu = 1.5$ , close to the dry-cutting  
 361 case. However, the flow modes in these two cases are very different—segmented (alkoxide)  
 362 versus sinuous (dry). The force reduction is due to the alkoxide layer on the initial workpiece  
 363 surface triggering repeated fracture and segmented flow. The force decrease is, however, not  
 364 as great as in the IPA cutting case; likewise the chip is also not as thin as in the laminar flow  
 365 case, compare **Figs. 7, 8**. Furthermore, segmented flow cannot be inferred from the force  
 366 trace alone, since this trace (**Fig. 10**) does not show any oscillations that might correspond  
 367 to the periodic cracks in the chip.

#### 368 4.5. Uniqueness of the Al-IPA system

369 The Al-IPA system is unique in that it can produce three of the four primary surface  
 370 flow modes in the same configuration, merely by varying the chemical environment. The  
 371 underlying reason for this is the reactivity of an oxide-free Al surface with alcohols as well as  
 372 the lubrication properties of the resulting alkoxide layer. In order to better demonstrate the  
 373 uniqueness of this configuration, two additional, secondary experiments were carried out.

#### 374 4.5.1. *Lubrication due to alkoxide film*

375 To emphasize the important role of the alkoxide film in effecting lubrication of the chip-  
376 tool interface, annealed Cu was cut under identical conditions to those described in Sec. 3  
377 for Al. It has been shown previously that the cutting characteristics of annealed Cu in dry  
378 cutting are very similar to those of Al under similar conditions: a sinuous flow mode prevails  
379 with very thick chip and large cutting force [10, 11].

380 Importantly, there is no report of any alkoxide-type layer occurring on freshly generated  
381 Cu surfaces. So any change in  $F_c$  with Cu, if observed, can only be attributed to presence  
382 of an IPA liquid film, devoid of alkoxide, in the tool-chip contact. **Figure 11** shows the  
383 variation of  $F_c$  in dry and IPA cutting of annealed Cu. The force is essentially the same  
384 in both cases indicating that the lubricating effect of the IPA, sans the alkoxide layer at  
385 the tool-chip interface, is negligible. Furthermore, it unambiguously points to the alkoxide  
386 layer as the cause for the large reduction in friction observed in the aluminum IPA cutting  
387 (Sec. 4.4).

388 Taken together, these results establish the key role of the alkoxide in reducing the friction  
389 force (drag) at the tool-chip contact when cutting Al. Equally importantly, this drag reduc-  
390 tion alters the flow mode in the primary deformation zone: the sinuous flow of dry cutting  
391 is replaced by a laminar flow mode in IPA cutting, with much smaller forces and energy  
392 consumption, and deformation strains. These latter attributes are also much desirable in  
393 practice.

#### 394 4.5.2. *Importance of the initial oxide layer*

395 The alkoxide cutting experiments established that the deformation can be influenced not  
396 just by alkoxide being present at the tool-chip interface, as in the IPA-cutting experiments,  
397 but also when it is present at the chip free surface. This result leads to a new hypothesis  
398 about the influence of the free surface in the IPA cutting experiment. Since the experiment  
399 is conducted in a medium of IPA, it is present at both the chip free surface and tool-chip  
400 interface and possibly influences the deformation from both surfaces. In order to exclude  
401 this possibility, the following secondary experiment was performed. An annealed Al work-  
402 piece, with natural surface oxide layer present, was immersed in IPA for 10 minutes at room

403 temperature and then allowed to air-dry completely by evaporation. Any possible reaction  
404 with the workpiece free surface should have occurred at this time and so influence subsequent  
405 deformation. This Al workpiece was then cut in the dry condition without application of  
406 IPA. Sinuous flow with a thick chip resulted, with an  $F_c \simeq 450\text{N}$ ; indistinguishable from  
407 the previous Al dry-cutting (see **Fig. 10**). This shows that the initial IPA application did  
408 not result in any alkoxide formation on the workpiece. This is as expected, since the in-  
409 herent oxide layer on the Al surface would prevent any chemical reaction with the alcohol.  
410 Therefore, in the case of IPA cutting, the formation of the alkoxide is solely restricted to the  
411 tool-chip interface and the new created (cut) workpiece surface; the free surface of the chip  
412 is chemically unaltered. Furthermore, the alkoxide is formed only when fresh Al is exposed  
413 to the alcohol by the cutting. This result validates the hypothesis that the results of the  
414 IPA-cutting experiment are purely due to lubrication at the tool-chip interface due to the  
415 presence of the alkoxide.

#### 416 *4.6. Surface quality*

417 The three flow modes—sinuous, laminar and segmentation—observed in the dry, IPA  
418 and alkoxide cutting experiments, respectively, also showed characteristic features on the  
419 macroscale. The most notable of these signatures were the forces and energy dissipation,  
420 just discussed, and quality of the final cut surface.

421 The quality of the cut surface is of interest from an applications standpoint, as it deter-  
422 mines component performance. The requirements on this surface usually include minimal  
423 density of defects such as cracks and tears, and small values of roughness. The three ambient  
424 conditions, with distinct flow modes and force levels, gave rise to surfaces with distinctly  
425 different properties.

426 The sinuous flow with folding, typical of dry cutting, resulted in a surface of poor quality  
427 (**Fig. 12(a)**). Optical profilometry of the cut surface for this flow condition revealed large  
428 tears/cracks; an example of such a tear is shown in **Fig. 12(a)**. Each of these tears often  
429 spanned the entire width of the cut. By examining large regions of the cut surface, the tears  
430 were estimated to occur at an average frequency of  $0.3/\text{mm}$ . This spacing is consistent with  
431 the oscillation frequency of the forces in dry cutting (see **Fig. 10**). The average depth of  
432 the tears (peak to valley distance) was  $\sim 430\ \mu\text{m}$ , which is much greater than  $h_0$ . While

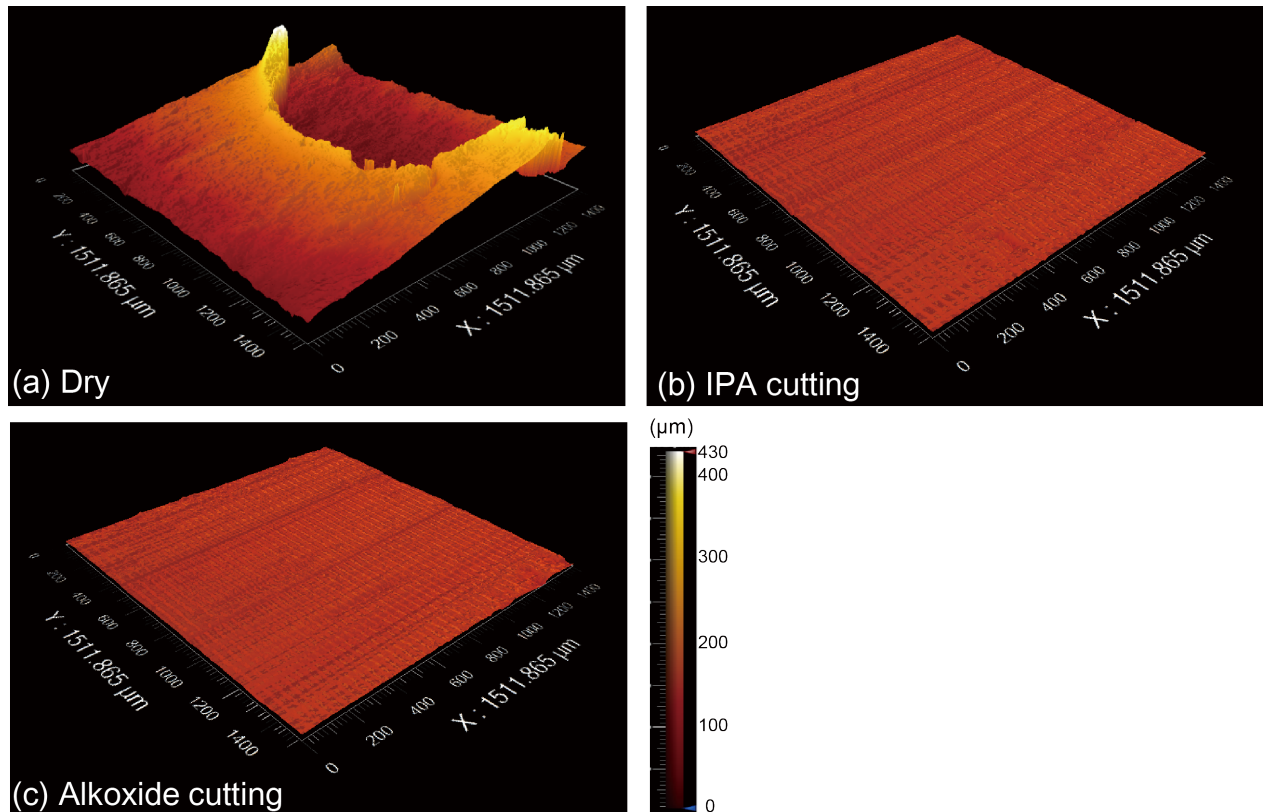


Figure 12: 3-D optical profilometer images of cut surface of Al showing topography and defect features. (a) Dry cutting—A surface defect in form of a tear is seen. (b), (c) In the case of IPA and alkoxide cutting, the quality of the cut surface is seen to be much better, with relatively smooth surface topography and absence of defects like the tears.



433 the mechanism of formation of these tears has not yet been resolved, it has been shown in  
434 a related sliding configuration [27] that the folds arising in sinuous flow nucleate defects by  
435 various types of fold-splitting in the wake of the tool/die. We envisage a similar mechanism  
436 herein, accentuated also by high  $F_f$ , in the sinuous flow mode, which inhibits easy flow of  
437 the chip against the tool face. No dead-metal or stagnation zones were observed on the tool  
438 rake face, thereby ruling them out as potential causes for the tears and cracks.

439 In sharp contrast to the dry cutting, both IPA cutting with laminar flow and alkoxide  
440 cutting with segmented flow resulted in much smoother cut surfaces; see **Figs. 12(b),(c)**.  
441 Firstly, there were very few, if any, tears and cracks on the surface. Secondly, the surface  
442 roughness,  $R_a$ , was  $1.75\ \mu\text{m}$  and  $1.80\ \mu\text{m}$  for the IPA and alkoxide cutting, respectively. The  
443 peak-to-valley distance was measured to be  $8.1\ \mu\text{m}$  and  $6.0\ \mu\text{m}$  respectively. The improvement  
444 in the finish, when compared to the dry-cutting, is more than an order of magnitude, even  
445 simply by comparing the peak-to-valley distance. This significant improvement in quality is  
446 undoubtedly a consequence of the corresponding flow modes, with resulting (much) smaller  
447 forces (**Fig. 10**).

## 448 5. Discussion

449 The high-speed *in situ* measurements in large-strain deformation of Al in the presence of  
450 isopropyl alcohol (IPA) have revealed an intricate link between surface plastic flow modes and  
451 the surrounding chemical environment. Based on the conditions (dry/IPA/alkoxide cutting),  
452 three distinct flow modes were produced in the same system without changing the workpiece  
453 material or deformation geometry. Transitions between the flow modes occurred purely due to  
454 a change in the chemical environment. These flow transitions were accompanied by large scale  
455 changes in the cutting forces, energy and deformation strain, as well as quantifiable changes  
456 in the properties of the cut surface. The occurrence of different flow modes was principally  
457 determined by the specific manner in which the IPA reacted with the Al surface—formation  
458 of an alkoxide film on the tool-chip interface vis-à-vis the workpiece free surface resulted in  
459 two completely different flow modes. In this context, the present mechanochemical effect is  
460 distinct from our recent report of a material-independent mechanochemical effect in metals  
461 [28]. In the latter case, a single flow transition—from sinuous to segmented—was observed

462 with a range of chemical media and with three different metal systems, the prerequisite being  
463 strong adhesion of the chemical medium to the metal surface [28]. The present results from  
464 the Al-IPA system highlight a mechanochemical effect that is material and chemical medium  
465 specific. The effect demonstrates a wider range of flow transitions, therefore, enabling one to  
466 more fundamentally probe the stability of plastic flow in large strain deformation as discussed  
467 below.

### 468 *5.1. Flow stability, plastic buckling and fracture*

469 The role of stability in determining the deformation mode is clearly exemplified in the  
470 case of sinuous flow. As shown in Sec. 4.1, this flow is initiated by a plastic buckling event on  
471 the workpiece surface just ahead of the tool/chip, leading to material folding. The buckling  
472 instability can be understood using a simplified model of a beam on a foundation representing  
473 the undeformed chip material ahead of the tool [11, 33]. Consequently, by considering the  
474 competition between material removal by homogeneous laminar flow and plastic deformation  
475 via buckling, the onset of sinuous flow can be predicted as a function of  $\alpha$  and initial material  
476 pre-strain  $\epsilon_{pre}$ . When buckling occurs, laminar flow becomes unstable and sinuous flow  
477 results.

478 Sinuous flow itself can become unstable in the presence of certain adsorptive chemicals  
479 at the free surface of the chip. In the case of alkoxide cutting, the presence of alkoxide on  
480 the uncut Al workpiece surface (**Fig. 3**) alters the flow from sinuous to segmented (Sec. 4.3).  
481 Segmentation is characterized by periodic and repeated cracks propagating from the chip  
482 free surface towards the tool tip (**Fig. 9**). Usually, segmentation is observed in metals which  
483 are relatively less ductile, when the plastic strain at the chip free surface reaches a critical  
484 value [38]. However, when segmentation is observed in annealed Al, it being a prototypical  
485 example of a highly ductile metal, there is a need for an alternative explanation.

486 The sudden transition from ductile to brittle behavior is reminiscent of stress-corrosion  
487 cracking and hydrogen embrittlement that is reported in structural metals, usually with  
488 disastrous consequences ensuing [16–18]. In the alkoxide cutting, it is likely that the chemi-  
489 cally adsorbed alkoxide layer effectively decreases the surface energy of the workpiece; such  
490 a decrease can lead to local embrittlement of the metal, in line with theoretical predictions  
491 [21, 53].

492 In addition to the surface energy reduction, the presence of notch-like features at the  
493 surface can create an environment conducive for crack propagation. **Figure 6** shows how  
494 the development of the initial buckle between two pinning points in sinuous flow leads to the  
495 formation of such features. In the presence of the alkoxide layer, a notch tip corresponding  
496 to one pinning point, becomes unstable to crack growth as opposed to continued plastic  
497 deformation. Consequently, the propagation of cracks from the pinning points makes sinuous  
498 flow an unstable flow mode and leads, instead, to segmented flow, as seen in **Fig. 9**. This type  
499 of transition is also a signature of a material-independent mechanochemical effect, wherein  
500 surface energy reduction via physical adsorption, coupled with pre-existing notch-like features  
501 on the surface, can drive crack growth [28].

502 On the other hand, the IPA cutting experiment (Sec. 4.2) provides evidence for an alter-  
503 nate route to alter stability of sinuous flow—if the forces at the tool-chip interface are reduced  
504 by the use of a suitable lubricating film, the compressive loading imposed on the plastic zone  
505 ahead of the chip also reduces. This indeed occurs with the IPA cutting, wherein the cutting  
506 and thrust forces are both reduced by an order of magnitude (**Fig. 10**). As a result, the  
507 buckling threshold force is shifted (increased) so that laminar flow becomes the more stable  
508 mode. Consequently, the metal demonstrates homogeneous laminar flow (**Fig. 7**). Here, the  
509 alkoxide layer at the tool-chip interface plays the role of the lubricating film.

510 In summary, sinuous flow transitions into laminar flow when the tool-chip interface is  
511 lubricated, and to segmented flow when a suitable chemical is adsorbed on the chip free  
512 surface. Both of these flow modes are characterized by much smaller forces and energy dissi-  
513 pation vis-à-vis the sinuous flow. Furthermore, in the presence of both these conditions, i.e.,  
514 tool-chip interface lubrication and an adsorbed layer on then free surface, the development  
515 of plastic buckling with folding is again prevented. Consequently, the notches necessary for a  
516 crack to propagate do not develop. Therefore, although the metal free surface energy might  
517 be altered due to the alkoxide, the absence of notch-like features on the surface preclude the  
518 possibility of crack propagation and segmented flow. This was confirmed experimentally by  
519 performing the alkoxide cutting in the presence of IPA, so that the alkoxide is present on  
520 both the free surface as well as the tool-chip interface. The resulting flow was laminar with  
521 no signs of any crack growth events.

522 *5.2. A phase diagram for stability of surface plastic flow*

523 The observations can now be presented in the form of a stability diagram for surface  
524 plastic flow modes, see **Fig. 13(a)**. Here the vertical axis is the initial pre-strain ( $\epsilon_{pre}$ ) in the  
525 workpiece and the horizontal axis is the deformation geometry (rake angle  $\alpha$ ). This figure  
526 represents a ‘phase diagram’ in that each point in the  $\epsilon_{pre} - \alpha$  plane corresponds to one  
527 particular experimental condition, i.e., specific pre-strain and geometry. In the absence of  
528 any plastic instabilities, the default flow mode, for any  $\epsilon_{pre}, \alpha$  is one of homogeneous strain,  
529 i.e., laminar flow (black circle). This figure also includes negative values for  $\alpha$ , with very  
530 large negative values corresponding to sliding without any chip formation.

531 The plastic buckling instability, leading to sinuous flow, can be incorporated into this  
532 diagram by using a simple model [33]. As a result, a critical  $\epsilon_{pre}(\alpha)$  relation is obtained—red  
533 dashed curve in **Fig. 13(a)**. For  $\epsilon_{pre}$  values that lie below this curve, the material buckles  
534 prior to laminar flow so that folding with sinuous flow ensues. This region of the  $\epsilon_{pre} - \alpha$   
535 diagram corresponds to situations where sinuous flow is the stable flow mode. Similarly, for  
536  $\alpha$  values above this curve, the cutting forces are sufficiently small that plastic buckling no  
537 longer occurs. In this region, laminar flow predominates, as is well known [13, 33].

538 On the other hand, segmented flow can be incorporated into the phase diagram by con-  
539 sidering the threshold for crack nucleation from the chip free surface. This curve (cyan in  
540 **Fig. 13(a)**) has the following characteristics, as derived from prior work [38]. Crack ini-  
541 tiation is usually favored in regions of high accumulated plastic strain. However, for large  
542 positive  $\alpha$ , the amount of pre-strain required for crack initiation is quite large, and under  
543 these conditions, only laminar flow occurs. For less-positive  $\alpha$ , the  $\epsilon_{pre}$  required for crack ini-  
544 tiation is smaller implying increased propensity for segmented flow. Consequently, the area  
545 of the phase diagram above the cyan curve corresponds to segmented flow—the experimental  
546 points (cyan circles) support this observation.

547 Finally, for completeness, the condition for shear band flow is also depicted (blue circle).  
548 Shear banding is a mode of flow localization, and is typical at very high  $\epsilon_{pre}$  ( $> 4.5$ ). The  
549 mechanics of shear band formation is, however, outside the scope of the present study and is  
550 discussed elsewhere [12, 54]

551 The stability phase diagram provides a basis for explaining the observed flow transitions.

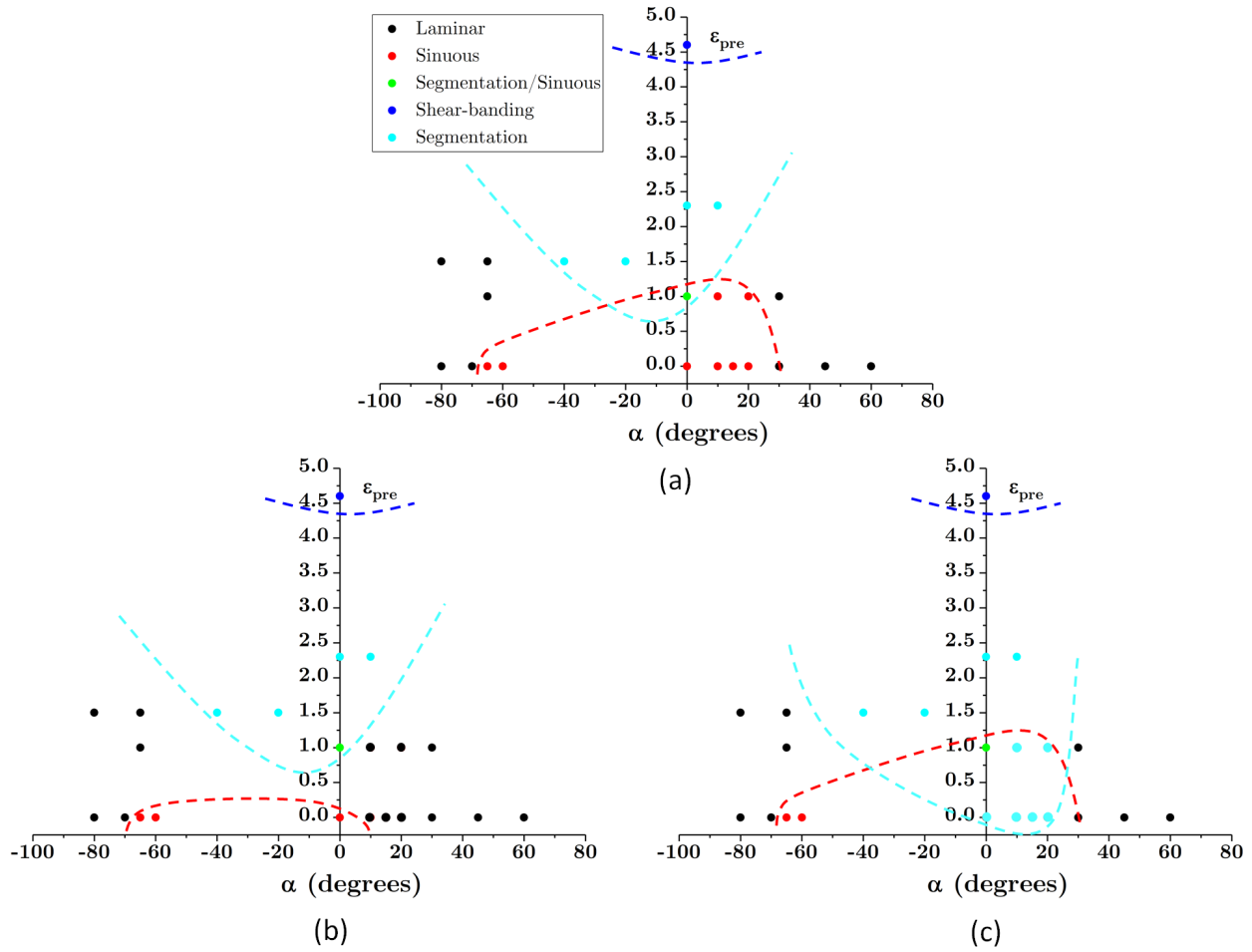


Figure 13: Phase diagram showing domains of stability of different plastic flow modes. A point in this diagram corresponds to a single experiment specified by deformation geometry (rake angle  $\alpha$ ) and initial deformation state (pre-strain,  $\epsilon_{pre}$ ) of the workpiece surface. (a) Phase diagram for dry cutting (no chemical environment) showing points with sinuous flow (red), laminar flow (black), segmented flow (cyan) and shear banding (blue). The buckling (red) and crack initiation (cyan) curves are also shown. (b) During IPA cutting, the buckling curve shifts downward due to lubrication by the alkoxide layer. This causes a flow transition from sinuous to laminar. (c) In the case of alkoxide cutting, the crack initiation curve shifts downward, resulting in a transition from sinuous to segmented flow.

- 552 • **IPA cutting:** Under these conditions, a lubricating film is present at the tool-chip  
553 interface. This film significantly reduces the propensity for plastic buckling, resulting  
554 in a transition from sinuous to laminar flow. Consequently, in **Fig. 13**, the buckling  
555 curve is shifted downward (red dashed line), see **Fig. 13(b)**. Now, points which initially  
556 resulted in sinuous flow (red circles) switch stability to laminar flow (black circles).
- 557 • **Alkoxide cutting:** In the presence of an alkoxide surface film, the workpiece surface  
558 energy is lowered. Correspondingly in **Fig. 13(c)**, the crack nucleation threshold curve  
559 (cyan) is shifted downward. In this case, even though plastic buckling is more stable  
560 than laminar flow, crack nucleation at pinning points represents an alternative stable  
561 mode. As a result, cracks now grow from the pinning points towards the tool tip  
562 leading to periodic segmentation (**Fig. 9**). Consequently, points that otherwise showed  
563 sinuous flow (red circles, part (a)) now demonstrate segmented flow (cyan circles) under  
564 identical  $\epsilon_{pre} - \alpha$  conditions.

565 The schematic diagram qualitatively explains the observations for a given initial starting  
566 condition. The same starting conditions in **Fig. 13(a)** switch stability in parts **(b)** and **(c)**  
567 due to changes in the buckling or crack initiation thresholds. However, additional exper-  
568 imental validation is necessary to establish the plastic buckling (red) and crack initiation  
569 (cyan) curves more quantitatively. This will involve further probing of the  $\epsilon_{pre} - \alpha$  space by  
570 performing a series of experiments with varying initial conditions. Furthermore, the diagram  
571 is likely to change depending on the material chosen (Al vs. Cu, for instance) and will have to  
572 be recomputed accordingly. However, this process can be accelerated by noting that *ex situ*  
573 or macroscale observations such as forces can distinguish certain flow modes, see **Fig. 10**,  
574 precluding the need for detailed *in situ* flow mapping.

### 575 5.3. Implications for processing applications

576 Fundamentally, the results show that surface plastic flow in large-strain, shear deformation  
577 can be varied by suitable modification of the chemical environment, suggesting routes for  
578 improving performance of machining and surface deformation processes. In particular, the  
579 observations strongly suggest that the chemical ambient environment in the deformation  
580 zone can be a useful variable for process control, over and beyond the usual process variables

581 such as deformation geometry and workpiece initial deformation state. From a technological  
582 standpoint, the results have two immediate implications. Firstly, the machining of many  
583 soft metals and/or highly strain-hardening metals (e.g., Al, Cu, Fe, Ni, Ta, stainless steels),  
584 notoriously referred to as being gummy and difficult to cut, could potentially be improved  
585 many-fold by use of a suitable chemical (or corrosive) effect either at the chip under-surface  
586 or at the workpiece free surface. For this purpose, the medium must be designed or tailored  
587 to effect a chemical reaction at one or more of these surfaces and interfaces. The process  
588 performance improvement is reflected in significantly reduced forces and energy dissipation  
589 (*cf.* **Fig. 10**), and improved surface quality (*cf.* **Fig. 12**). The reduced specific energy  
590 will also result in lower temperatures in the deformation zone, with additional benefits to  
591 workpiece surface quality and tool wear. Secondly, the chemical medium can be tailored  
592 to the metal, via its effect on the initial workpiece surface, as has been demonstrated in  
593 the alkoxide cutting. In many machining, surface generation and forming processes, the  
594 workpiece free surfaces are quite readily accessed by chemical media; whereas lubrication of  
595 the tool/die-workpiece contact is much more difficult due to limits imposed by the intimate  
596 and severe nature of this contact, a consequence of large contact pressures and elevated  
597 temperatures imposed by the tool. In fact, such surface phenomena are already beginning to  
598 find use for improved efficiency in material processing [55]. Thus attractive possibilities exist  
599 for a new class of mechanochemically-assisted cutting and deformation processes for metals,  
600 akin to those developed for non-metals, that exploit surface chemistry principles.

601 The results also have scientific implications. Firstly, the use of chemical media may  
602 provide a route for studying surface plastic flow modes and stability of this plastic flow  
603 systematically. Secondly, it points to critical areas where current modeling of large strain  
604 deformation in metal cutting and deformation processes needs improvement. One of these  
605 is the friction boundary condition at the tool-chip contact in lubricated cutting. The IPA  
606 cutting results conclusively show that this boundary condition cannot just be described via  
607 use of a Coulomb-type friction coefficient, with a smaller value than in dry cutting, as is  
608 often done. The other critical area pertains to incorporating flow stability criteria (e.g.,  
609 buckling, segmentation) and microstructure in continuum models of metal cutting. For this  
610 is necessary to predict unsteady flow modes like sinuous and segmented flows, and the flow

611 transitions that have been demonstrated. Lastly, the mechanochemical effect highlighted  
612 herein is intriguing in that its manifestation is coupled to the occurrence of unsteady flow  
613 modes like sinuous flow in metals. We plan to elaborate on some of these topics and questions  
614 in future work.

## 615 **6. Conclusions**

616 A study has been made of the development of surface plastic flow in large-strain defor-  
617 mation of metals in the presence of a chemically active medium. Using high-speed, *in situ*  
618 imaging observations of simple shear deformation in a model system—plane-strain cutting of  
619 soft annealed aluminum in an isopropyl alcohol (IPA) environment—the occurrence of three  
620 distinct plastic flow modes is demonstrated. All of these flow modes are manifest in the  
621 same material depending on details of IPA application, under otherwise identical conditions  
622 of deformation geometry and initial workpiece state (annealed). Transitions between these  
623 modes are effected by the nature of the chemical environment—a mechanochemical effect.

624 In dry cutting, absent the chemical medium, the flow mode is (non-laminar) sinuous flow  
625 characterized by surface plastic buckling and large-amplitude folding. The corresponding  
626 strain field is highly non-homogeneous with large deformation strains and very high forces,  
627 even though the material being sheared is quite soft. However, when the shear deformation is  
628 imposed in the presence of the IPA, two fundamentally distinct plastic flow modes are seen—  
629 segmented flow distinguished by crack propagation from the free surface of the metal (chip  
630 free surface) and non-homogeneous straining; and laminar flow with a smooth homogeneous  
631 strain field. Both of these flow modes are characterized by small deformation (cutting)  
632 forces and specific energy—almost an order of magnitude smaller than with the sinuous  
633 flow—effected by reduced straining. The change in flow mode in the presence of the IPA  
634 is shown to result from the reaction between the IPA and freshly generated Al surfaces,  
635 the latter a product of the deformation. When the IPA application is tailored to create an  
636 alkoxide layer on the workpiece free surface ahead of the tool, the ductility of the surface layer  
637 is lowered—local embrittlement—with periodic crack nucleation and propagation from this  
638 surface resulting in the segmented flow. In contrast, when the IPA action is tailored to create  
639 a highly effective lubricant film (most likely an alkoxide layer) on the chip under-surface in



640 the tool-chip contact region, the resulting lowering of the imposed forces suppresses plastic  
641 buckling and sinuous flow. Instead laminar flow, with much smaller deformation strains,  
642 results. The mechanochemical effect highlighted herein is shown to be strongly coupled to  
643 the nucleation of the sinuous flow, distinguishing it from other flow and fracture phenomena  
644 in surface plasticity such as liquid metal embrittlement and stress corrosion cracking.

645 The occurrence of different flow modes and flow transitions, and the coupling between  
646 the mechanochemical effect and sinuous flow, are explained in the framework of plastic flow  
647 stability. In this framework, the stability boundaries are altered by the action of the chemical  
648 medium on the metal surface thereby creating conditions for crack nucleation or establishing  
649 laminar flow. The work suggests interesting opportunities, exploiting the mechanochemical  
650 effect, for much improved cutting of soft and highly strain-hardening metals like copper, iron,  
651 nickel and stainless steels— materials often termed ‘gummy’ because of the difficulty involved  
652 in their cutting.

## 653 **Acknowledgement**

654 The authors would like to acknowledge support from NSF grants CMMI 1562470 and  
655 DMR 1610094.

## 656 **References**

- 657 [1] C. Zener, in *Fracturing of Metals* (American Society for Metals, Cleveland, Ohio, 1948)  
658 pp. 3–31.
- 659 [2] R. Hill, The mechanics of machining: a new approach, *J. Mech. Phys. Solids* **3**, 47 (1954).
- 660 [3] J. R. Rice, in *Proceedings of the 14th International Congress on Theoretical and Applied*  
661 *Mechanics*, ed. *W. T. Koiter* (North-Holland, Amsterdam, 1976) pp. 207–220.
- 662 [4] P. Dewhurst, On the non-uniqueness of the machining process, *Proceedings of the Royal*  
663 *Society of London A: Mathematical, Physical and Engineering Sciences* **360**, 587 (1978).
- 664 [5] R. F. Recht, Catastrophic thermoplastic shear, *J. Appl. Mech.* **31**, 189 (1964).

- 665 [6] J. G. Ramsay and M. I. Huber, *Modern Structural Geology, Volume 2: Folds and Frac-*  
666 *tures* (Academic Press, London, 1987).
- 667 [7] T. J. Burns and M. A. Davies, Nonlinear dynamics model for chip segmentation in  
668 machining, *Phys. Rev. Lett.* **79**, 447 (1997).
- 669 [8] B. Dodd, S. M. Walley, R. Yang, and V. F. Nesterenko, Major steps in the discovery  
670 of adiabatic shear bands, *Metallurgical and Materials Transactions A* **46**, 4454 (2015).
- 671 [9] L. Dai, M. Yan, L. Liu, and Y. Bai, Adiabatic shear banding instability in bulk metallic  
672 glasses, *Appl. Phys. Lett.* **87**, 141916 (2005).
- 673 [10] H. Yeung, K. Viswanathan, W. D. Compton, and S. Chandrasekar, Sinuous flow in  
674 metals, *Proceedings of the National Academy of Sciences* **112**, 9828 (2015).
- 675 [11] H. Yeung, K. Viswanathan, A. Udupa, A. Mahato, and S. Chandrasekar, Sinuous flow  
676 in cutting of metals, *Phys. Rev. Appl* **8**, 054044 (2017).
- 677 [12] K. Viswanathan, A. Udupa, H. Yeung, D. Sagapuram, J. B. Mann, M. Saei, and  
678 S. Chandrasekar, On the stability of plastic flow in cutting of metals, *CIRP Annals-*  
679 *Manufacturing Technology* **66**, 69 (2017).
- 680 [13] M. C. Shaw, *Metal Cutting Principles* (Oxford University Press, 2005).
- 681 [14] F. P. Bowden and D. Tabor, *Friction: An Introduction to Tribology* (RE Krieger Pub-  
682 lishing Company, 1973).
- 683 [15] R. M. Latanision and R. H. Jones, *Chemistry and Physics of Fracture* (Martinus Nijhoff  
684 Publishers, 1987).
- 685 [16] W. Rostoker, J. McCaughey, and H. Markus, *Embrittlement by Liquid Metals* (Reinhold  
686 Pub. Corp., 1960).
- 687 [17] W. D. Robertson, *Stress Corrosion Cracking and Embrittlement* (J. Wiley, New York,  
688 1956).

- 689 [18] O. Reynolds, Chem. news 29, 117-118 (1874); mem, Proceedings of the Literary and  
690 Philosophical Society of Manchester **13**, 93 (1874).
- 691 [19] P. Rehbinder, New physico-chemical phenomena in the deformation and mechanical  
692 treatment of solids, Nature **159**, 866 (1947).
- 693 [20] E. D. Shchukin, The influence of surface-active media on the mechanical properties of  
694 materials, Adv. Colloid Interface Sci. **123**, 33 (2006).
- 695 [21] J. R. Rice, in *Chemistry and Physics of Fracture*, edited by R. M. Latanision and R. H.  
696 Jones (Martinus Nijhoff, Boston, 1987, 1987) pp. 23–44.
- 697 [22] R. M. Latanision, in *Surface Effects in Crystal Plasticity*, edited by R. M. Latanision  
698 and J. T. Fourie (Nordhoff, Leyden, 1977) pp. 3–48.
- 699 [23] A. R. C. Westwood and J. J. Mills, in *Surface Effects in Crystal Plasticity*, edited by  
700 R. M. Latanision and J. T. Fourie (Nordhoff, Leyden, 1977) pp. 835–862, see also dis-  
701 cussion by A. Argon, following the article.
- 702 [24] N. P. Suh, The delamination theory of wear, Wear **25**, 111 (1973).
- 703 [25] K. Johnson, Contact mechanics and the wear of metals, Wear **190**, 162 (1995).
- 704 [26] J. M. Challen, L. J. McLean, and P. L. B. Oxley, Plastic deformation of a metal surface  
705 in sliding contact with a hard wedge: its relation to friction and wear, Proceedings of  
706 the Royal Society of London A: Mathematical, Physical and Engineering Sciences **394**,  
707 161 (1984).
- 708 [27] A. Mahato, Y. Guo, N. K. Sundaram, and S. Chandrasekar, Surface folding in metals:  
709 a mechanism for delamination wear in sliding, Proceedings of the Royal Society A **470**,  
710 20140297 (2014).
- 711 [28] A. Udupa, K. Viswanathan, M. Saei, J. B. Mann, and S. Chandrasekar, Material-  
712 independent mechanochemical effect in the deformation of highly-strain-hardening met-  
713 als, Phys. Rev. Appl **10**, 014009 (2018).

- 714 [29] P. A. Rehbinder and E. D. Shchukin, Surface phenomena in solids during deformation  
715 and fracture processes, *Prog. Surf. Sci.* **3**, 97 (1972).
- 716 [30] K. H. Brown, D. A. Grose, R. C. Lange, T. H. Ning, and P. A. Totta, Advancing the  
717 state of the art in high-performance logic and array technology, *IBM J. Res. Dev.* **36**,  
718 821 (1992).
- 719 [31] Y. Namba and H. Tsuwa, Mechanism and some applications of ultra-fine finishing, *CIRP*  
720 *Annals-Manufacturing Technology* **27**, 511 (1978).
- 721 [32] M. Krishnan, J. W. Nalaskowski, and L. M. Cook, Chemical mechanical planarization:  
722 slurry chemistry, materials, and mechanisms, *Chem. Rev.* **110**, 178 (2009).
- 723 [33] A. Udupa, K. Viswanathan, Y. Ho, and S. Chandrasekar, The cutting of metals via  
724 plastic buckling, *Proceedings of the Royal Society A* **473**, 20160863 (2017).
- 725 [34] M. E. Merchant, Mechanics of the metal cutting process. I. Orthogonal cutting and a  
726 type 2 chip, *J. Appl. Phys.* **16**, 267 (1945).
- 727 [35] R. Komanduri and B. Von Turkovich, New observations on the mechanism of chip for-  
728 mation when machining titanium alloys, *Wear* **69**, 179 (1981).
- 729 [36] K. Nakayama, in *Proceedings of International Conference on Production Engineering*  
730 (1974) pp. 572–577.
- 731 [37] W. A. Backofen, Deformation processing, *Metallurgical Transactions* **4**, 2679 (1973).
- 732 [38] Y. Guo, W. D. Compton, and S. Chandrasekar, In situ analysis of flow dynamics and  
733 deformation fields in cutting and sliding of metals, *Proceedings of the Royal Society A*  
734 **471**, 20150194 (2015).
- 735 [39] A. R. C. Westwood, Tewksbury lecture: Control and application of environment-  
736 sensitive fracture processes, *J. Mater. Sci.* **9**, 1871 (1974).
- 737 [40] K. Dao and D. Shockey, A method for measuring shear-band temperatures, *J. Appl.*  
738 *Phys.* **50**, 8244 (1979).

- 739 [41] D. Bradley, Metal alkoxides, Progress in Inorganic Chemistry, Volume 2 , 303 (1960).
- 740 [42] O. Helmboldt, L. Keith Hudson, C. Misra, K. Wefers, W. Heck, H. Stark, and M. Dan-  
741 ner, Aluminum compounds, inorganic, in *Ullmann's Encyclopedia of Industrial Chem-*  
742 *istry* (Wiley-VCH Verlag GmbH & Co. KGaA, 2000) p. 578.
- 743 [43] J. Gladstone and A. Tribe, I.aluminium alcohols. part i. their preparation by means of  
744 the aluminium-iodine reaction, J. chem. Soc. Trans. **39**, 1 (1881).
- 745 [44] R. Montgomery, The effect of alcohols and ethers on the wear behavior of aluminum,  
746 *Wear* **8**, 466 (1965).
- 747 [45] M. C. Shaw, Action of n-primary alcohols as metal cutting fluidsalternating properties  
748 with chain length, J. Am. Chem. Soc. **66**, 2057 (1944).
- 749 [46] S. Hironaka and T. Sakurai, The effect of pentaerythritol partial ester on the wear of  
750 aluminum, *Wear* **50**, 105 (1978).
- 751 [47] F. P. Bowden and D. Tabor, *The Friction and Lubrication of Solids (Oxford Classic*  
752 *Texts in the Physical Sciences)* (Oxford University Press, 2001).
- 753 [48] C. Kajdas, About an anionic-radical concept of the lubrication mechanism of alcohols,  
754 *Wear* **116**, 167 (1987).
- 755 [49] K. Strawhecker, D. Asay, J. McKinney, and S. Kim, Reduction of adhesion and friction  
756 of silicon oxide surface in the presence of n-propanol vapor in the gas phase, *Tribol. Lett.*  
757 **19**, 17 (2005).
- 758 [50] J. E. Williams, E. F. Smart, and D. R. Milner, Metallurgy of machining. Part 1: Basic  
759 considerations and the cutting of pure metals, *Metallurgia* **81**, 3 (1970).
- 760 [51] V. Piispanen, Theory of formation of metal chips, *J. Appl. Phys.* **19**, 876 (1948).
- 761 [52] E. Lee and B. Shaffer, The theory of plasticity applied to a problem of machining, *J.*  
762 *Appl. Mech.* **18**, 405 (1951).

- 763 [53] J. R. Rice and R. Thomson, Ductile versus brittle behaviour of crystals, *Philos. Mag.*  
764 **29**, 73 (1974).
- 765 [54] D. Sagapuram, K. Viswanathan, A. Mahato, N. K. Sundaram, R. M'Saoubi, K. P.  
766 Trumble, and S. Chandrasekar, Geometric flow control of shear bands by suppression  
767 of viscous sliding, *Proceedings of the Royal Society A* **472**, 20160167 (2016).
- 768 [55] T. Sugihara, Y. Nishimoto, and T. Enomoto, On-machine tool resharpening process  
769 for dry machining of aluminum alloys employing lme phenomenon, *Precis. Eng.* **40**, 241  
770 (2015).